

Non-magnetic tight binding disorder effects in the γ sheet of Sr_2RuO_4

P. Contreras^a, D. Osorio^a, and Sh. M. Ramazanov^b

^a*Departamento de Física, Universidad de Los Andes, Mérida 5101, Venezuela,*

^b*Department of Physics, Dagestan State University, Makhachkala, Russia*

Received 13 September 2021; accepted 6 October 2021

Inspired by the physics of the Miyake - Narikiyo model (MN) for superconductivity in the γ sheet of Sr_2RuO_4 , we set out to investigate numerically the behavior caused by a non-magnetic disorder in the imaginary part of the elastic scattering matrix for an anisotropic tight-binding model. We perform simulations by going from the Unitary to the Born scattering limit, varying the parameter c which is inverse to the strength of the impurity potential. It is found that the unitary and intermedia limits persist for different orders of magnitude in simulating the disorder concentration. Subsequently and in order to find the MN tiny gap, we perform a numerical study of the unitary limit as a function of disorder concentration, to find the tiny anomalous gap.

Keywords: Unconventional superconductivity; triplet reversal time broken state; γ sheet; Sr_2RuO_4 ; non-magnetic disorder; elastic scattering cross-section; tiny gap.

DOI: <https://doi.org/10.31349/RevMexFis.68.020502>

1. Introduction

Strontium ruthenate (Sr_2RuO_4) is a body-centered tetragonal crystal with a layered square structure for the ruthenium atoms [1]. Its normal state is described by a Fermi liquid, with three metallic conduction sheets in the Fermi surface (FS), namely the α , β , and γ sheets [2]. In addition, Sr_2RuO_4 is an unconventional superconductor with $T_c \approx 1.5$ K that strongly depends on non-magnetic disorder [3]. From the beginning, it was proposed that Sr_2RuO_4 is an unconventional superconductor with triplet pairing and some type of nodes in the order parameter for each sheet of the FS [4], where the symmetry of the superconducting gap is believed to break time reversal symmetry [5-7].

Although some authors consider that the γ sheet of the FS does not have nodes, several low temperature works have provided experimental agreement with nodes in the specific heat $C(T)$, the electronic heat transport $\kappa_i(T)$ and directional ultrasound $\alpha_j(T)$ measurements. These measurements resemble some kind of nodes on the FS including the γ sheet (see [8] and references therein for a review of the experiments with the first crystal samples of Sr_2RuO_4). Recently, novel experimental and theoretical advances continue to be carried out in the comprehension of the broken time-reversal symmetry superconducting state of Sr_2RuO_4 . All recent and old studies continue to be crucial in order to explain the microscopic mechanism inherent to superconductivity in this compound ([9-12] and references there in).

In this work, we use a tight binding nearest neighbor expression for $\xi_\gamma(k_x, k_y)$ in order to model the γ sheet, which is centered at (0,0) in the first Brillouin zone, $\xi_\gamma(k_x, k_y) = -\epsilon + 2t[\cos(k_x a) + \cos(k_y a)]$ with hopping parameters $(t, \epsilon) = (0.4, 0.4)$ meV, and electron-hole symmetry. For the k dependence of the gap, we use the 2D tight binding expression corresponding to the Miyake-Narikiyo model

[13] for a triplet state in the γ sheet, that is, $\hat{\Delta}^\gamma(k_x, k_y) = \Delta_0 d^\gamma(k_x, k_y)$, with the vector $d^\gamma(k_x, k_y) = [(\sin(k_x a) + i \sin(k_y a))\hat{z}]$ and $\Delta_0^\gamma = 1.0$ meV, in impurity samples [3] (the issue of tuning Δ_0^γ will be considered separately).

The nine points where the order parameter (OP) $\hat{d}^\gamma(k_x, k_y)$ has zeros are sketched in Fig. 1, that is, 4 points symmetrically distributed in the 10 and 01 planes at k -points $(0, \pm\pi)$ and $(\pm\pi, 0)$, 4 points symmetrically distributed in the 11 planes at k -points $(\pm\pi, \pm\pi)$ and 1 point in the 00 plane at k -point $(0,0)$.

As noticed in Ref. [13], the gap on the γ sheet is very anisotropic and leaves a tiny gap around $(0, \pm\pi)$ and $(\pm\pi, 0)$ points. According to group theory considerations, the imaginary OP has two components which belong to the irreducible representation E_{2_u} of the tetragonal point group D_{4h} . It corresponds to a triplet odd paired state $\hat{d}^\gamma(-k_x, -k_y) = -\hat{d}^\gamma(k_x, k_y)$ with basis functions $\sin(k_x a)$ and $\sin(k_y a)$ and

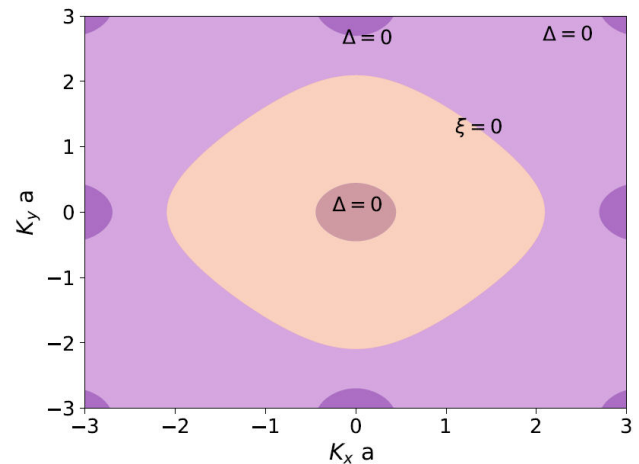


FIGURE 1. 2D implicit plot of the tight binding anisotropic Fermi γ sheet $\xi_\gamma(k_x, k_y) = 0$ and the triplet superconducting gap with the localization of the nine points where $\hat{d}^\gamma(k_x, k_y) = 0$.

Ginzburg-Landau coefficients (1,*i*) [14,16]. The 3D analogous to the MN model is the Zhitomirski and Rice (ZR) interband model [17], however the ZR model has nodes on the 3 sheets of the FS, contrary to the MN model, since the OP zeros do not touch the γ sheet, but are closed to it (tiny gap model).

In the following sections, we briefly report a visual numerical analysis of the MN model for the γ sheet on Sr_2RuO_4 at the phenomenological level (the microscopy mechanism is explained in their work [13]). We use a particular methodology [16]. First we vary the inverse strength parameter c from 0 to 1 and second, we vary the value of the parameter Γ^+ from optimal to dilute doping in the function $\tilde{\omega}(\omega + i0^+)$. We finish our short report by comparing our findings with a line nodes tight binding analysis for High Tc compounds recently investigated using the same approach [18].

2. From the unitary to the Born limit in triplet superconductors

We introduce the main equation for the elastic scattering involving the self-energy $\tilde{\omega}(\omega + i0^+)$ in the case of non-magnetic disorder according to [16] by following their approach to model experimental low temperature data in the unitary region, where the hydrodynamic limit does not work. The dressed $\tilde{\omega}(\omega + i0^+)$ can be written in the following way

$$\tilde{\omega}(\omega + i0^+) = \omega + i\pi\Gamma^+ \frac{g(\tilde{\omega})}{c^2 + g^2(\tilde{\omega})}. \quad (1)$$

Equation (1) describes the self-consistent renormalization in energy due to elastic scattering of superconducting pairs on non-magnetic atoms for the case of electron-hole symmetry in unconventional superconductors, *i.e.* $g(\tilde{\omega}) = g_0(\tilde{\omega})$ (we omit the γ label in the main equations). The parameter $c = 1/(\pi N_F U_0)$ is the inverse of the impurities strength, N_F is the Fermi level DOS, and U_0 is the impurity potential. The parameter $\Gamma^+ = n_{\text{imp}}/(\pi^2 N_F)$ is proportional to the impurity concentration n_{imp} . Non-magnetic disorder assumes N equal scatters randomly distributed, but independent each other, it also assumes that on a macroscopic scale, the crystal is homogeneous [19]. The effect of non-magnetic disorder in Sr_2RuO_4 is to suppress superconductivity states around nodal/quasi-nodal regions. The function $g(\tilde{\omega})$ in (1) is given by

$$g(\tilde{\omega}) = \left\langle \frac{\tilde{\omega}}{\sqrt{\tilde{\omega}^2 - |\Delta|^2(k_x, k_y)}} \right\rangle_{FS},$$

and the average over the γ sheet of the $FS \langle \dots \rangle_{FS}$ is performed with the tight binding expressions mentioned in the introduction, and according a numerical technique successfully used to fit experimental low temperatures ultrasound data with an accidental 3D point nodes model similar to the ZR model [20-22].

Finally, if electron-hole symmetry is not considered on the γ sheet, the other spin Pauli components $g^\gamma(\tilde{\omega})$ have to be taken into consideration, that is, $g_1^\gamma(\tilde{\omega})$ and $g_3^\gamma(\tilde{\omega})$, but for a p-wave triplet gap $g_1^\gamma(\tilde{\omega}) \sim d^\gamma(k_x, k_y)_{FS} = 0$, and $g_3^\gamma(\tilde{\omega}) \sim d_\xi(k_x, k_y)_{FS} = 0$, Born's approximation applies and if $c \gg 1$ (*i.e.* $U_0 \ll 1$) with a new disorder doping parameter $\Gamma_B^+ = \Gamma^+/c^2 \ll 1$, however we do not expect Born scattering to play a role in the low temperature properties in this compound for the γ sheet. This is because any small amount of non-magnetic dirt can be in principle provided by local Sr atoms, and will cause the γ sheet of Sr_2RuO_4 to be in the unitary limit, or to be close to it. The imaginary part of (1) defines the inverse of the quasiparticle disordered averaged lifetime $\tau^{-1}(\omega)$ as

$$\tau^{-1}(\omega) = 2\Im[\tilde{\omega}(\omega + i0^+)]. \quad (2)$$

In the unitary limit, $\tau^{-1}(\omega)$ has a resonance at zero frequency, that is, $\tilde{\omega}(0) = i\gamma$, where γ defines the "impurity averaged" zero energy elastic scattering rate [15], and determines the crossover energy scale separating the two scattering limits. Since we expect normal state excitations in energy (provided by very small amounts of non-magnetic local Sr atoms) to be less than γ , self-consistency in Eq. (1) cannot be neglected. Finally we refer the readers to [23] for an extended treatment of the theoretical formalism for non magnetic impurity scattering in unconventional superconductors, and to [24] for a recent review on impurity effects and modelling techniques. The impurity effect with unitary scattering was also investigated in Refs. [25-30]. Finally, for Fermi and Bose atomic gases at ultra-cold temperatures in the unitary limit see [31]. If instead of investigating the tiny gap region, we set up the region where the gap Δ in magnitude is bigger than frequency ω , the main effect in $\tilde{\omega}(\omega + i0^+)$ is to shift the real part by an amount proportional to $\omega - \Gamma^+ \Delta/\tilde{\omega}$ which tends to zero as the dressed frequency value $\tilde{\omega}$ is increased.

In this section, we compute the solution of Eq. (1) by varying the parameter inverse to the strength c , and by fixing the value of disorder concentration Γ^+ for two cases of physical interest. The first case is for a value of $\Gamma^+ = 0.3$ meV, which resembles optimally doped values of impurities in experimental samples. The second case is for a dilute disorder concentration n_{imp} , that is, $\Gamma^+ = 0.05$ meV. In Sr_2RuO_4 , Sr atoms in the lattice form an additional impurity level in the energy zone, thus, Sr atoms are part of the structure and also are the centers on which non-magnetic elastic scattering occurs.

Figure 2 shows the evolution of $\Im[\tilde{\omega}(\omega + i0^+)]$ as function of the parameter c which is inversely proportional to the strength U_0 , going from strong $U_0 \gg 1$ ($c \rightarrow 0$) (violet curve) to values $U_0 \ll 1$ ($c \rightarrow 1$) (yellow curve) *i.e.* when $\pi N_F U_0 \rightarrow 1$, ($N_F \sim 10^{15} \text{ eV}^{-1}$) or an electron-hole symmetric tight binding dispersion and for an optimal disorder concentration $\Gamma^+ = 0.3$ meV. The region under $\Im[\tilde{\omega}(\omega + i0^+)]$ in the unitary limit which corresponds to a resonance at zero frequency has been shaded violet in the

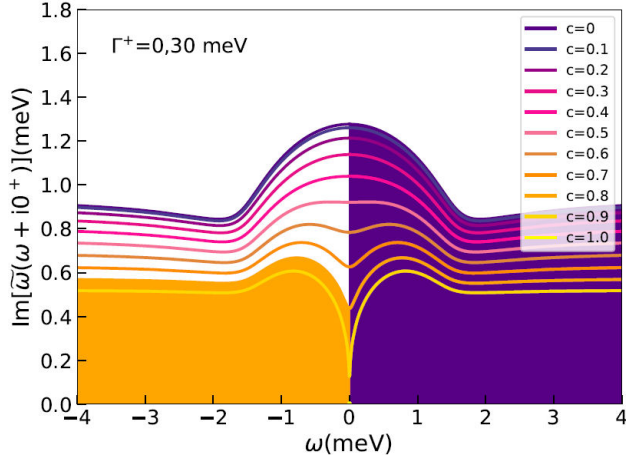


FIGURE 2. Evolution of the imaginary part of the scattering matrix from the unitary limit to intermediate regions for a value $\Gamma^+ = 0.30$ meV.

right side of the plot. On the other hand, a well-defined intermediate scattering region with a finite minimum at zero frequencies, and resonances at $\omega \sim \pm 0.8$ meV, which correspond to an inverse strength of $c = 1$ has been shaded orange in the left side. We observe the unitary behavior from $c = 0$ to $c = 0.5$, and well-defined intermediary regions from $c = 0.6$ up to values $c = 1$, that is, $U_0 \rightarrow \pi^{-1} N_F^{-1}$.

In Fig. 2, non-magnetic disorder affects most strongly the low energy region up to 1.5 meV. We also see from Fig. 2 that in the normal state, for energies bigger than the gap value, the function $\Im[\tilde{\omega}](\omega + i0^+)$ becomes constant, but tends to depend on the c value.

Figure 3 shows the evolution of $\Im[\tilde{\omega}](\omega + i0^+)$ as a function of c for a dilute concentration of impurities, that is, $\Gamma^+ = 0.05$ meV. The $c = 0.1$ region for $\Im[\tilde{\omega}](\omega + i0^+)$ in the unitary limit has been shaded blue in the right side of the plot. We observe a much smaller ‘‘impurity averaged’’ zero energy elastic scattering rate ($\gamma \sim 0.05$ meV) than in the previous case ($\gamma \sim 1.3$ meV).

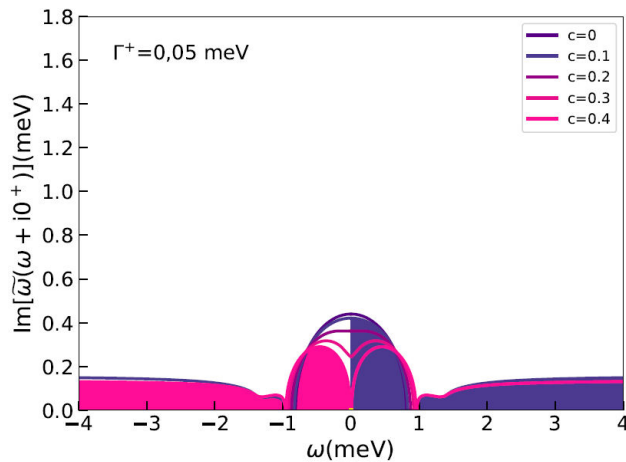


FIGURE 3. Evolution of the imaginary part of the scattering matrix from the unitary limit to intermediate regions for a value $\Gamma^+ = 0.05$ meV.

Finally we observe in Fig. 3, an anomalous drop to zero of the function $\Im[\tilde{\omega}](\omega + i0^+)$ around $\omega \sim 1.0$ meV for the five values of c where the solution was found. Therefore, in the next section we study the unitary limit $c = 0$ in order to further investigate into that anomaly.

3. Inside the unitary limit, the visualization of the Miyake Narikiyo tinny gap in the γ sheet

In this section, we visualize the behavior of $\Im[\tilde{\omega}](\omega + i0^+)$ inside the unitary limit ($c = 0$) for different values of the impurities concentration parameter Γ^+ , starting at very dilute disorder (yellow line), to an optimal disorder (violet line). For large values of U_0 , the unitary limit in Eq. (1) is given by expression

$$\tilde{\omega}(\omega + i0^+) = \omega + i\pi\Gamma^+ \frac{1}{g(\tilde{\omega})}. \quad (3)$$

The unitary regime is defined as the limit where the elastic scattering due to non-magnetic disorder is so strong that the mean-free path becomes comparable to the Fermi momentum k_F , meanwhile in the Born metallic limit, the mean free path is much larger than the Fermi momentum k_F . This means that normal state quasiparticles in the unitary region have an ill-defined momentum between elastic collisions. In this formalism, the signature of the unitary state is the resonance at zero frequency in the imaginary part of the scattering matrix.

Figure 4 shows the evolution of $\Im[\tilde{\omega}](\omega + i0^+)$ according to Eq. (3), and for nine values of Γ^+ . We observe the smooth resonance centered at zero frequency for all values, with smaller values of residual zero energy γ for very dilute values of disorder Γ^+ . The region for $\Im[\tilde{\omega}](\omega + i0^+)$ corresponding to an optimal levels of disorder, $\Gamma^+ = 0.4$ meV, has been shaded violet in the right side of the plot. In addition, the region corresponding to dilute levels of disorder with

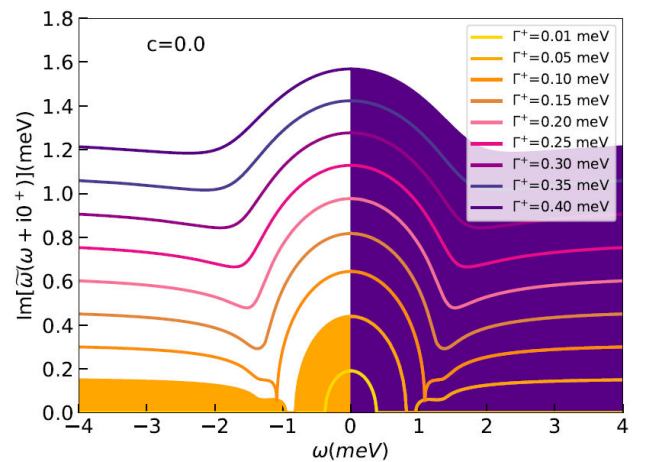


FIGURE 4. Evolution of the imaginary part of the scattering matrix inside the unitary limit for nine values of the parameter Γ^+ (meV).

$\Gamma^+ = 0.05$ meV, has been shaded yellow in the left side of the figure.

In the left part of the Fig. 4, the MN tiny gap, that was numerically observed by using a density of states DOS analysis, is found in the $\Im[\tilde{\omega}](\omega + i0^+)$ analysis as well. The tiny gap is given by $\Im[\tilde{\omega}](\omega + i0^+) = 0$ and is found in the interval between 0.85 meV and 1.0 meV, corresponding to a 15% of the value $\Delta_0 = 1.0$ meV used. This tiny gap effect in the function $\Im[\tilde{\omega}(\omega + i0^+)] \sim \tau^{-1}(\omega)$ will have significance for the low temperature transport properties since it enters the expressions for several kinetic coefficients.

In order to compare the results, we performed an analysis using the same methodology for a lines nodes tight binding model for a High T_c materials [16]. It allows us to state, that the case of the γ sheet tight binding analysis on Sr_2RuO_4 , is much more sensitive to strong elastic scattering events and self consistency at low temperatures, since the unitary limit persists for most of the values used for the modeling parameters c and Γ^+ .

4. Conclusions

This communication was aimed at investigating numerically the behavior of the elastic scattering non-magnetic disordered averaged matrix $\tilde{\omega}(\omega + i0^+)$ for a MN 2D anisotropic tight binding model for the γ sheet of Sr_2RuO_4 . In Sec. 2, we modeled and visualized the behavior of the imaginary part

$\Im[\tilde{\omega}](\omega + i0^+)$ of the scattering matrix. The dependence on the inverse of the strength of the disorder potential U_0 , *i.e.* the parameter c , was studied for two regions of physical importance, an optimal disorder region with $\Gamma^+ = 0.4$ meV, and a dilute region with $\Gamma^+ = 0.05$ meV. The results were illustrated in Figs. 2 and 3.

We found that the function $\Im[\tilde{\omega}](\omega + i0^+)$ is always within the unitary or intermedia scattering limits for the values of the parameters used, contrasting with the case of a High T_c modeling where the Born hydrodynamic limit is present at small values of the parameter c [17]. In Sec. 3, the behavior of the disordered matrix $\tilde{\omega}(\omega + i0^+)$ inside the unitary ($c = 0$) region was studied for nine values of Γ^+ , starting at very diluted disorder, optimal disorder values, and finally an enriched disorder.

The results were visualized in Fig. 4, the tiny MN gap was found for a $\Gamma^+ = 0.05$ meV in disorder concentration. We end this short note pointing out that the MN model is very useful for setting up numerical studies in triplet superconductors such as strontium ruthenate, as we have demonstrated in this study.

Acknowledgements

The authors did not receive financial support for research, authorship and/or publication of this article.

-
1. Y. Maeno *et al.*, Superconductivity in a layered perovskite without copper, *Nature* **372** (1994) 532, <https://doi.org/10.1038/372532a0>.
 2. C. Bergemann, A. P. Mackenzie, S. R. Julian, D. Forsythe, E. Ohmichi, Quasi-two-dimensional Fermi liquid properties of the unconventional superconductor Sr_2RuO_4 , *Advances in Physics* **52** (2003) 639, <https://doi.org/10.1080/00018730310001621737>.
 3. M. Suzuki, M. A. Tanatar, N. Kikugawa, Z. Q. Mao, Y. Maeno, and T. Ishiguro, Universal Heat Transport in Sr_2RuO_4 , *Phys. Rev. Lett.* **88** (2002) 227004, <https://doi.org/10.1103/PhysRevLett.88.227004>.
 4. T. M. Rice and M. Sigrist, Sr_2RuO_4 : an electronic analogue of ^3He ?, *Journal of Physics: Condensed Matter* **7** (1995) L643, <https://doi.org/10.1088/0953-8984/7/47/002>.
 5. K. Ishida *et al.*, Spin-triplet superconductivity in Sr_2RuO_4 identified by ^{17}O Knight shift, *Nature* **396** (1998) 658, <https://doi.org/10.1038/25315>.
 6. G. M. Luke *et al.*, Time-reversal symmetry-breaking superconductivity in Sr_2RuO_4 , *Nature* **394** (1998) 558, <https://doi.org/10.1038/29038>.
 7. J. A. Duffy, S. M. Hayden, Y. Maeno, Z. Mao, J. Kulda, and G. J. McIntyre, Polarized-Neutron Scattering Study of the Cooper-Pair Moment in Sr_2RuO_4 *Phys. Rev. Lett.* **85** (2000) 5412, <https://doi.org/10.1103/PhysRevLett.85.5412>.
 8. A. P. Mackenzie and Y. Maeno, The superconductivity of Sr_2RuO_4 and the physics of spin-triplet pairing, *Rev. Mod. Phys.* **75** (2003) 657, <https://doi.org/10.1103/RevModPhys.75.657>.
 9. C. W. Hicks *et al.*, Strong Increase of T_c of Sr_2RuO_4 Under Both Tensile and Compressive Strain, *Science* **344** (2014) 283, <https://doi.org/10.1126/science.1248292>.
 10. S. Benhabib *et al.*, Ultrasound evidence for a two-component superconducting order parameter in Sr_2RuO_4 , *Nat. Phys.* **17** (2021) 194, <https://doi.org/10.1038/s41567-020-1033-3>.
 11. S. Ghosh *et al.*, Thermodynamic evidence for a two-component superconducting order parameter in Sr_2RuO_4 , *Nat. Phys.* **17** (2021) 199, <https://doi.org/10.1038/s41567-020-1032-4>.
 12. V. Grinenko *et al.*, Unsplit superconducting and time reversal symmetry breaking transitions in Sr_2RuO_4 under hydrostatic pressure and disorder. *Nat. Commun.* **12** (2021) 3920, <https://doi.org/10.1038/s41467-021-24176-8>.
 13. K. Miyake and O. Narikiyo, Model for Unconventional Superconductivity of Sr_2RuO_4 : Effect of Impurity Scattering on Time-Reversal Breaking Triplet Pairing with a Tiny Gap, *Phys. Rev. Lett.* **83** (1999) 1423, <https://doi.org/10.1103/PhysRevLett.83.1423>.

14. M. B. Walker and P. Contreras, Theory of elastic properties of Sr_2RuO_4 at the superconducting transition temperature, *Phys. Rev. B* **66** (2002) 214508, <https://doi.org/10.1103/PhysRevB.66.214508>.
15. P. Contreras, J. Florez and R. Almeida, Symmetry Field Breaking Effects in Sr_2RuO_4 , *Rev. Mex. Fis.* **62** (2016) 442,
16. E. Schachinger and J. P. Carbotte, Residual absorption at zero temperature in d-wave superconductors, *Phys. Rev. B* **67** (2003) 134509, <https://doi.org/10.1103/PhysRevB.67.134509>.
17. M. E. Zhitomirsky and T. M. Rice, Interband proximity effect and nodes of superconducting gap in Sr_2RuO_4 , *Phys. Rev. Lett.* **87** (2001) 057001, <https://doi.org/10.1103/PhysRevLett.87.057001>.
18. P. Contreras, D. Osorio, Scattering Due to Non-magnetic Disorder in 2D Anisotropic d-wave High Tc Superconductors, *Engineering Physics* **5** (2021) 1, <https://doi.org/10.11648/j.ep.20210501.11>.
19. J. M. Ziman, Models of Disorder: The Theoretical Physics of Homogeneously Disordered Systems, (Cambridge University Press, Cambridge, 1979).
20. P. Contreras, M. Walker, and K. Samokhin, Determining the superconducting gap structure in from sound attenuation studies below T_c , *Phys. Rev. B* **70** (2004) 184528, <https://doi.org/10.1103/PhysRevB.70.184528>.
21. P. Contreras, Electronic heat transport for a multiband superconducting gap in Sr_2RuO_4 , *Rev. mex. fis.* **57** (2011) 395,
22. P. Contreras, *et al.*, A numerical calculation of the electronic specific heat for the compound Sr_2RuO_4 below its superconducting transition temperature. *Rev. Mex. Fis.* **60** (2014) 184,
23. V. P. Mineev and K. Samokhin, Introduction to Unconventional Superconductivity, (Amsterdam, Gordon and Breach Science Publishers, 1999).
24. Y. G. Pogorelov, V. M. Loktev, Conventional and unconventional impurity effects in superconductors, *Low Temperature Physics*, **44** (2018) 1, <https://doi.org/10.1063/1.5020892>.
25. P. J. Hirschfeld, P. Wolfe, and D. Einzel, Consequences of resonant impurity scattering in anisotropic superconductors: Thermal and spin relaxation properties, *Phys. Rev. B* **37** (1988) 83, <https://doi.org/10.1103/PhysRevB.37.83>.
26. K. Maki and H. Won, Why d-wave superconductivity?, *Journal de Physique I* **6** (1996) 2317, <https://doi.org/10.1051/jp1:1996220>.
27. L. S. Borkowski, P.J. Hirschfeld, and W.O. Putikka, Transport properties of extended-s-state superconductors, *Phys. Rev. B* **52** (1995) R3856, <https://doi.org/10.1103/PhysRevB.52.R3856>.
28. C. J. Pethick and D. Pines, Transport processes in heavy-fermion superconductors, *Phys. Rev. Lett.* **57** (1986) 118, <https://doi.org/10.1103/PhysRevLett.57.118>.
29. S. Schmitt-Rink, K. Miyake, and C. M. Varma, Transport and Thermal Properties of Heavy-Fermion Superconductors: A Unified Picture, *Phys. Rev. Lett.* **57** (1986) 2575, <https://doi.org/10.1103/PhysRevLett.57.2575>.
30. A. V. Balatsky, M. I. Salkola, and A. Rosengren, Impurity-induced virtual bound states in d-wave superconductors, *Phys. Rev. B* **51** (1995) 15547, <https://doi.org/10.1103/PhysRevB.51.15547>.
31. L. P. Pitaevskii, Superfluid Fermi liquid in a unitary regime, *Phys.-Usp.* **51** (2008) 603, <https://doi.org/10.1070/PU2008v051n06ABEH006548>.